A physical model of tropical cyclone central pressure filling at landfall

Nathan Sparks* and Ralf Toumi

Imperial College London, London, UK.

**Corresponding author*: Nathan Sparks, nsparks@ic.ac.uk

ABSTRACT

We derive a simple physically based analytic model which describes the pressure filling of a tropical cyclone (TC) over land. Starting from the axisymmetric mass continuity equation in cylindrical coordinates we derive that the half-life decay of the pressure deficit between the environment and TC centre is proportional to the initial radius of maximum surface wind speed. The initial pressure deficit and column-mean radial inflow speed into the core are the other key variables. The assumptions made in deriving the model are validated against idealised numerical simulations of TC decay over land. Decay half-lives predicted from a range of initial TC states are tested against the idealized simulations and are in good agreement. Dry idealised TC decay simulations show that without latent convective heating, the boundary layer decouples from the vortex above leading to a fast decay of surface winds while a mid-level vortex persists.

1. Introduction

The behaviour of a tropical cyclone (TC) in the hours after it makes landfall is critical in determining its hazardous potential. Various modelling experiments and analyses have been used to gain insight into the factors affecting decay at landfall. A set of modelling experiments which test the response of an idealized TC to various levels of instantaneous surface roughening and drying is performed by Chen and Chavas (2020). However, the dependence on the initial state of the TC was not examined. Hlywiak and Nolan (2021) perform realistic landfall simulations and finds that surface wind decay sensitivity to surface roughness is dependent on the intensity and size of the TC as it decays although only one initial case is tested. Trends of reduced land-induced decay rates have also been reported for the US (Li and Chakraborty 2020) and globally (Phillipson and Toumi 2021). Li and Chakraborty (2020) attribute this to warming SSTs via increased TC moisture content but determine that TC size does not affect the wind speed decay rate.

Batts et al. (1980) were among the first to examine the rate of decay of TCs after making landfall. They proposed a filling model for the central pressure, linear in time, and independent of the initial TC state. Among the first to examine the factors affecting the rate of pressure filling after landfall were Jarvinen et al. (1985) who found that the largest decreases in intensity occurred within the first six hours of the most intense storms making landfall and assumed a quadratic fill rate of central pressure. Ho et al. (1987) developed upon this showing that more intense TCs tend to fill faster while also noting that there is a dependence of size on intensity in their database of landfalling TCs. They do not attempt to separate the contributions from the two variables to the filling rate largely due to a scarcity of data. Vickery and Twisdale (1995) quantified the above observations by assuming an exponential decay model for central pressure deficit with a decay constant proportional to the initial deficit. Vickery (2005) extend this analysis to include TC size dependence and find that the decay rate is also inversely proportional to the radius of maximum wind in a study of many historical landfalling hurricanes. The intensity is diagnosed via the central pressure deficit, the difference between the environmental and central pressure, which is empirically assumed to decay exponentially. The TC size dependence of the decay rate is attributed to the rate at which a significant fraction of the storm area becomes affected by land as a storm moves over land. Kaplan and Demaria (1995) and DeMaria et al. (2006) identify translation speed and distance inland as key parameters controlling decay with later iterations considering the fraction of the circulation over land. The basis of these models is that the decay rate of $Vmax$ is proportional to $Vmax$ itself which leads to exponential decay of $Vmax$ with a time constant. However, these empirical assumptions of exponential decay for both $Vmax$ and pressure deficit and size dependence lack a physical framework. Chen and Chavas (2021) show that existing intensification theory may be adapted to predict the decay of surface winds in idealized landfall simulations and Phillipson and Toumi (2021) show that a physically based algebraic model for $Vmax$ fits global observations of landfall decay. These theories do not consider the role of size.

Here we attempt to provide a physical basis for the pressure filling at landfall by proposing an analytic solution to the mass continuity equation in the tropical cyclone core. We demonstrate, through a set of numerical simulations, that the inner-core size and the radius of surface maximum wind speed are important physical variables which control the rate of the pressure deficit decay over land. We support this finding with a simple new analytical physically based framework which suggests the half-life of the central pressure deficit is proportional to the size of the inner-core of a decaying TC.

2. Physical filling model

When a TC makes landfall the increased surface friction combined with reduced surface enthalpy fluxes quickly leads to a net transport of mass towards the TC centre reducing the central pressure deficit by ‘filling’ it with air. We develop a simple new framework in order to understand some of the dynamics of this filling process and ultimately gain understanding into key factors affecting the rate at which this occurs. We model the TC as an axisymmetric vortex and consider only horizontal motion as this contributes to surface pressure tendency. The integral form of the mass continuity equation in axisymmetric cylindrical polar coordinates for a cylinder of radius r is,

$$\frac{\partial \mathcal{M}}{\partial t} = -2\pi r \int \rho v_r \, \mathrm{d}z, \tag{1}$$

where $\mathcal{M}$ is the total mass of air within the cylinder, ρ is the density at radius r and height z, and v_r is the radial wind at radius r and height z. The average surface pressure within the cylinder is,

$$\langle P(r) \rangle = \frac{\mathcal{M} g}{\pi r^2} \tag{2}$$

where the angled brackets denote an average within radius r and g is the gravitational constant. We define $\mathcal{V}_r$ as the density-weighted column mean radial wind velocity at radius r,

$$\mathcal{V}_r = \frac{\int \rho v_r \, \mathrm{d}z}{\int \rho \, \mathrm{d}z}. \tag{3}$$

During TC decay, in the vicinity of the inner core, $\mathcal{V}_r$ is negative (directed toward the centre), filling the pressure deficit. Since the surface pressure, P, at a given radius is given by,

$$P(r) = g \int \rho \, \mathrm{d}z, \tag{4}$$

we can write the tendency of the average pressure within a cylinder of radius r as,

$$\frac{\partial \langle P(r) \rangle}{\partial t} = \frac{g}{\pi r^2} \frac{\partial M}{\partial t} = -\frac{2P(r)\mathcal{V}_r(r)}{r}. \tag{5}$$

The tendency of the central pressure, P_c, is then,

$$\frac{\mathrm{d}P_c}{\mathrm{d}t} = \lim_{r \to 0} \frac{\partial \langle P \rangle_r}{\partial t} = \lim_{r \to 0} -\frac{2P(r)\mathcal{V}_r(r)}{r} \tag{6}$$

and since $\mathcal{V}_r$ must tend to zero as r tends to zero to avoid infinite central pressure tendency, and invoking L'Hôpitals's rule,

$$\lim_{r \to 0} \frac{\mathcal{V}_r(r)}{r} = \lim_{r \to 0} \frac{\partial \mathcal{V}_r(r)}{\partial r} \tag{7}$$

giving,

$$\frac{\mathrm{d}P_c}{\mathrm{d}t} = -2P_c \lim_{r \to 0} \frac{\partial \mathcal{V}_r(r)}{\partial r} \tag{8}$$

We now make the assumption that the gradient of $\mathcal{V}_r$, evaluated at the central limit, may be linearised:

$$\lim_{r \to 0} \frac{\partial \mathcal{V}_r}{\partial r} = \frac{\chi}{Rmax_0} \tag{9}$$

where $Rmax_0$ is the radius of maximum wind speed at $t = 0$ and χ is the density-weighted column mean radial wind speed at $Rmax_0$ ($\chi = \mathcal{V}_r(Rmax_0)$) which we refer to as the 'column speed' and will typically have a negative sign (directed towards the centre). It is not immediately obvious that this linear gradient approximation is appropriate and this assumption will be examined later in section 2. It is important to note that we do not require $Rmax$ to be constant throughout the decay, as χ is defined at the initial $Rmax$, $Rmax_0$. We only require that $\mathcal{V}_r$ is linear in r out to $Rmax_0$ throughout the decay. It is also worth highlighting that this is the point at which the size of the TC core is introduced explicitly via $Rmax_0$. The fundamental quantity controlling the central pressure tendency in Equation 8 is the radial gradient of column speed but here we are effectively parameterising this single quantity in terms of two independent terms, the column speed and the initial size of the core. This separation is motivated by the fact that during TC decay the column speed must tend to zero as the TC fills while the core size may remain finite. This technique is useful because we may then parameterise the decay of the core column speed in terms of the central pressure deficit (Equation 12), ultimately allowing us to express the central pressure tendency as a function of central pressure itself and other parameters (Equation 13). $Rmax_0$ is simply a convenient scaling parameter we used to define the size of the TC core. The model is not sensitive to this choice as long as the above linearity assumption remains valid because χ is defined as $\mathcal{V}_r$ at $Rmax_0$ and always appears in a ratio with $Rmax_0$. This is also true of the precise definition of $Rmax$ itself. We validate the model here using $Rmax$ defined as the radius of maximum 10-m winds and show the linearity assumption is valid for this case. Alternative choices of $Rmax$, and indeed core size, may be valid but would require similar testing of the linearity assumption.

Combining Equations 8 and 9 gives the following formula for the central pressure tendency,

$$\frac{\mathrm{d}P_c}{\mathrm{d}t} = -\frac{2P_c\chi}{Rmax_0} \tag{10}$$

It is convenient to introduce a quantity we call the central pressure deficit fraction, $\tilde{P}$, defined by

$$\tilde{P} = \frac{P_e - P_c}{P_e} \tag{11}$$

where P_e is the environmental pressure. We then make a further assumption that χ decays as $\tilde{P}^k$,

$$\frac{\chi}{\chi_0} = \left(\frac{\tilde{P}}{\tilde{P}_0}\right)^k, \tag{12}$$

where k is a positive constant to be determined, $\tilde{P}_0$ is the initial central pressure deficit fraction and χ_0 is the initial column speed. A relationship of this form is proposed as under decay conditions we expect the mass flux towards the centre to be related to the frictional inflow in the boundary layer and the secondary circulation above the boundary layer. In both cases the pressure gradient force is the driver. We may expect that the secondary circulation driven by latent heating also includes upper level outflow and that this may decrease k. This will be verified later. The precise nature of this relationship including the value of k however is complex and related to the physics governing inflow and outflow speeds which we do not attempt to disentangle in this simple model. The assumed relationship in Equation 12 and the value of k is examined in section 2.

Combining Equations 10, 11, 12, and we can write the central pressure deficit fraction tendency as,

$$\frac{\mathrm{d}\tilde{P}}{\mathrm{d}t} = \frac{2\chi_0}{\tilde{P}_0^k Rmax_0}(\tilde{P}^k - \tilde{P}^{k+1}), \tag{13}$$

For small central pressure deficit fractions ($\tilde{P} \ll 1$, all k) we can make the approximation,

$$\frac{\mathrm{d}\tilde{P}}{\mathrm{d}t} \approx \frac{2\chi_0}{\tilde{P}_0^k Rmax_0}\tilde{P}^k \tag{14}$$

which can be integrated to give an analytical model for the decay of $\tilde{P}$ as a function of time,

$$\tilde{P}(t) = \tilde{P}_0 \left[1 + (k-1)\alpha t\right]^{\frac{1}{1-k}} \tag{15}$$

where α is a decay rate (dimensions of inverse time) defined by

$$\alpha = -\frac{2\chi_0}{\tilde{P}_0 Rmax_0}. \tag{16}$$

It should be noted that for the special case of $k = 2$, Equation 15 simplifies to an algebraic decay form and in the limit $k = 1$, the decay is exponential,

$$\tilde{P}(t) = \tilde{P}_0 \mathrm{e}^{-\alpha t}. \tag{17}$$

Equation 15 then yields an estimate of the central pressure deficit half-life in terms of k and the initial state parameters,

$$\hat{t}_{1/2} = -\frac{\tilde{P}_0 Rmax_0}{2\chi_0}\beta(k), \tag{18}$$

$$\beta(k) = \frac{2^{k-1} - 1}{k-1}. \tag{19}$$

The half-life therefore depends on three TC state variables: the core size, the initial pressure deficit and the column speed. Interestingly, although the form of the decay for $k = 1$ is exponential, the initial condition, $\tilde{P}_0$, also appears in the decay constant, and therefore the half-life. We note that the value of k will affect the magnitude of the half-life but not its dependence on the three TC state variables.

The above model makes two primary assumptions: i) the column-integrated inflow speed is linear in r from the centre until $Rmax$, and ii) the core column-integrated speed χ decays as $\tilde{P}^k$.

These assumptions allow us to express the time dependent pressure deficit fraction as a function of the initial pressure deficit fraction, radius of maximum wind, core column speed and k. From this the decay half-life is derived in terms of the same parameters. Of the four model parameters only two are readily observable. Obtaining good estimates of $\tilde{P_0}$ and $Rmax_0$ through observations may be realistic for real world landfalling TCs. The same cannot be said for χ_0 which is not easily evaluated even in numerical simulations. This is largely because it is a small difference between large inflow and outflow terms. However, we show that the model may potentially be useful without direct estimates of χ_0 per TC. It maybe possible to parameterise χ_0 in terms of other, more readily available physical quantities. Similarly, k is not a directly observable quantity, but we show the model may be useful regardless.

3. Methods

a. Simulation Setup

TC simulations are performed using the Weather Research and Forecasting (WRF) model, version 4.0 (Skamarock et al. 2019). Three nested square domains with two-way interaction are used. The outer domain has a side of length 7200 km (600 × 600 grid cells, 12 km grid spacing) and contains the middle domain with side length 3208 km (802 × 802 grid cells, 4 km grid spacing) which in turn contains the inner domain with a side length of 1069 km (802 × 802 grid cells, 1.333 km grid spacing). The time steps for the domains are 60 s, 20 s and 10 s respectively on an f-plane at 30°N which is representative of a typical landfall latitude. Each domain has 41 vertical levels of which about 12 are below 2 km height. The initial environmental conditions and lateral boundary conditions are given by the Jordan Mean Tropical Sounding during hurricane seasons (Jordan 1958). There is no background wind and a horizontal "sponge layer" with a width of 240 km absorbs noise along the outer domain boundaries by reducing the horizontal wind velocities to zero. A full suite of physics parameterisations are used and include the WRF single-moment 6-class microphysics scheme (Hong and Lim 2006), the Rapid Radiative Transfer Model for general circulation models (RRTMG) scheme (Iacono et al. 2008) for shortwave and longwave radiation, the Mellor–Yamada–Janjic (MYJ) planetary boundary layer scheme (Janjic 1994), and the Eta Similarity surface layer scheme (Janjic 2002). Given that the 4 km grid size middle domain is large enough to contain most of the structure of the simulated TCs no cumulus scheme is used in any domain.This idealised setup is also described in Wang and Toumi (2019).

b. Experiment Design

We first create a "Spin-up" run which provides TCs with range of initial states from which we can simulate land-induced decay. The Spin-up run is initialized with a bogus vortex, which is inserted in the centre of the domains and has an analytic wind profile (Wang and Toumi 2016) with a near-surface maximum wind speed of 18 m s^{-1} and a radius of maximum wind speed of 100 km with a wind speed which decreases linearly to zero from the surface to the WRF top at 20 km. The Spin-up TC is allowed to develop and mature over 15 days with the entire domain over an ocean surface with fixed SST of 29°C.

We then create a set of land-induced TC decay experiments from the Spin-up run by restarting the simulation with the ocean surface replaced by land over the entire domain. We perform these restart runs beginning two days into the Spin-up run, then every day until 14 days, which gives 13 experiment cases which we refer to as the "Control" experiments. These are labelled according the time in the Spin-up run at which they were started. The land surface type in these experiments is designated "croplands" in the Modified IGBP Modis 20-category land-use data set (Friedl et al. 2010) and has a roughness length, z_0, of 0.15 m. Soil moisture and temperature was not fixed. An additional set of experiment cases labelled "Dry" was created by repeating the above method, but at the point of restart, as well as replacing ocean with land, we also remove all moisture from the atmosphere and set surface moisture fluxes to 0 for the duration of the run to keep the atmosphere dry (Li and Chakraborty 2020).

The Dry experiments serve multiple purposes. They provide a way to simplify the decay process by removing latent heating allowing us to focus on the effect of surface frictional forcing. They also allow us to estimate the contribution of latent heating to the maintenance of the TC during the decay. Finally, they offer a way of testing our new analytic decay framework across TCs decaying in extremely different environments.

All simulation variables in the decay experiments were output and stored at hourly intervals at $t = 0, 1, 2 \ldots$ etc. hours. The density-weighted column-integrated radial wind speed, or "column speed", $\mathcal{V}_r$, was found to be unreliable when evaluated directly using instantaneous model output via Equation 3. We believe this is due to a combination of factors. Typical values for $\mathcal{V}_r$ in the vicinity of $Rmax$ are very small (~0.01 m s^{-1}) and are the residual or large inflow and outflow speeds (~10 m s^{-1}) so small fractional errors during the calculation lead to large fractional errors in the net flow. The coordinate system staggering in the numerical model, where the wind velocity components and pressure use coordinate systems offset from each other, is a further source of error especially in regions with large horizontal (especially radial) gradients of pressure and wind speed. We found that averaging the calculated values of $\mathcal{V}_r$ over the course of the decay provided only a marginal improvement in their numerical stability. We therefore employ Equation 5 to calculate $\mathcal{V}_r$ at hourly intervals halfway between the output time steps where $\frac{\partial \langle P \rangle_r}{\partial t}$ is evaluated as a finite central difference. $\mathcal{V}_r$ and therefore χ are then available at times $t = 0.5, 1.5, 2.5 \ldots$ etc. hours. All values of $\mathcal{V}_r$ and χ reported here are calculated using this method. In order to have TC state variables which are temporally aligned, the central pressure deficit fraction, $\tilde{P}$, and radius of maximum wind,

$Rmax$ are both evaluated at these times ($t = 0.5, 1.5, 2.5\ldots$ etc. hours) by linear interpolation from their on-the-hour values. We note that it may be possible to calculate a stable $\mathcal{V}_r$ over shorter time scales in this way but we found that hourly resolution was sufficient to effectively resolve the decay behaviour in these experiments. We acknowledge that evaluating $\mathcal{V}_r$ via Equation 5 rather than its first definition in Equation 3 introduces an element of circularity, since the initial pressure tendency is required to calculate χ_0 which then, via Equation 15, provides the time dependent form of the central pressure deficit fraction. We cannot therefore consider the model fully 'predictive' when $\mathcal{V}_r$ is evaluated as above.

The parameter k is evaluated by regression from $\tilde{P}$ and the inferred values of χ using Equation 12. Since this cannot be observed or calculated from initial conditions it is also a non-predictive parameter.

Given that the model depends on both observable ($Rmax_0, \tilde{P}_0$) and non-observable (χ_0, k) parameters we test the performance in stages to investigate the sensitivity of its performance to the non-observable quantities. We begin by estimating χ_0 and k per experiment and evaluating the time dependent performance and half-life given by the model. Then we use a constant k equal to the mean k across the experiments calculated in the previous step to evaluate performance. Finally we test the performance using a constant mean k and a constant mean χ_0. This final test is the fairest test of the model's predictive skill since it uses only observable quantities.

4. Results

a. Simulations Overview

An overview of the Spin-up run and the Control and Dry case experiments is shown in Figure 1. The idealized "Spin-up" TC initially contracts and intensifies during the first four days with the central pressure deficit fraction, $\tilde{P}$, reaching 0.12 and maximum azimuthally averaged 10 m wind speed, $Vmax$, reaching 69 m s^{-1} at a radius, $Rmax$, of 19 km. Following this $Vmax$ decays relatively quickly over the next three days to 45 m s^{-1}, then slowly until the end of simulation at 15 days to 39 m s^{-1}. $\tilde{P}$ behaves similarly, falling to 0.071 at 7 days then 0.062 at the end of the simulation. During this period of decay the TC grows approximately linearly with $Rmax$ reaching over 77 km by the end of the simulation.

We focus our analysis on the first 12 hours of the Control and Dry sets of land-induced decay experiments as in most cases this is long enough for $\tilde{P}$ to decay to half its initial value. During this period both $\tilde{P}$ and $Vmax$ decay in an exponential-like manner. In the Dry cases $Rmax$ tends to decrease to half its initial value over this period whereas $Rmax$ is more stable in the Control cases. In the Dry experiments, after eight hours $Rmax$ tends to increase noisily.

Analysis of the decay of $\tilde{P}$ reveals that the behaviour during the first hour of the experiments is qualitatively different to the hours following. During the first hour many cases experience a “shock" of transient deepening pressure deficit but then all cases decay monotonically and relatively smoothly. This phenomenon occurs in both Control and Dry sets of experiments but is more prominent in the Dry cases. We do not further examine this “shock" response here and in all following analysis ‘Initial’ values of TC parameters ($\tilde{P}_0$, $Rmax_0$, and χ_0) refer to their values evaluated at 1.5 h after land is imposed in the numerical experiments. We note that the “shock" response may be shorter than one hour, but allowing for one hour was sufficient in all cases to ensure subsequent decay was monotonic and smooth. Initial shock responses in $Vmax$ have been previously observed by Chen and Chavas (2020) in their surface roughening experiments. In our experiments $Vmax$ always decreased over the first hour. Initial parameter values, both $t = 0$ h and $t = 1.5$ h, for all experiments are provided in Table 1. $\tilde{P}$ takes longer to respond and in some experiments increases during the first hour. This decoupling of the central pressure from the surface winds limits the applicability of pressure-wind relationships originally inferred over the ocean (and justified by cyclostrophic balance) during landfall.

b. Control Experiments

The half-life of the land-induced decay simulations is the time taken for $\tilde{P}$ to decay to half of its initial value, calculated using piecewise linear interpolation. The mean half-life for the Control runs was 10.5 hours. The half-life for each decay case is shown in Table 1. Following Vickery (2005) we plot the exponential decay coefficient as a function of initial central pressure deficit, ΔP_0, divided by initial radius of maximum wind speed, $Rmax_0$, for the Control experiments in Figure 2. We compare our decay coefficients with their values in the Gulf coast and Florida Peninsular regions because they have a large range of $Rmax_0$ which give better estimates of the dependence of decay coefficient on $Rmax_0$ (Vickery 2005). Our simulated decay coefficients are similar to the weighted average of their Gulf coast and Florida Peninsular values and show a similar dependence on $Rmax_0$ divided by ΔP_0. We also show the weighted average of all regions which deviated further from our simulations.

The decay half-life is shown as a function of initial TC parameters in Figure 3 for the Control cases. The half-life is strongly correlated with $Rmax_0$ with an R^2 value of 0.76 (p-values < 0.001). $\tilde{P}_0$ is not significantly correlated (at the 95% confidence level) with half-life ($R^2 = 0.27$, p-value = 0.07). Excluding case 2 results in $\tilde{P}_0$ becoming significantly anti-correlated (at the 95% confidence level) with half-life. A large range of half-life values is observed with very similar values of $\tilde{P}_0$ for the sets of cases initialized during the slow decay of the spin-up TC (from day 7 onwards). χ_0 is uncorrelated with half-life in the Control cases.

1) Model performance

The physical pressure filling framework developed in section 2 permits an estimation of decay half-life, $\hat{t}_{1/2}$, using Equation 18 from initial TC state variables, $\tilde{P}_0$, $Rmax_0$, χ_0, and k. We first use values of χ_0, and k estimated for each experiment to calculate the model half-life and compare these the to simulation half-life (Figure 3d). The model and simulation values are very highly correlated with an R^2 value of 0.96 and and RMSE of 1.1 h. There is a mean positive bias in the model estimates of 0.8 h. We then use a constant k equal to the mean value of k for the Control experiments ($\overline{k} = 1.30$) and perform the same comparison (Figure 3e). Model estimated half-life is still strongly correlated with simulation half-life with an R^2 value of 0.82. The RMSE is 1.8 hours and the bias is slightly larger at 0.94 h. We can even make a further simplification by assuming both a constant (mean across cases) k and χ_0 ($\overline{\chi_0} = -0.026$ m s^{-1}) which gives $R^2 = 0.69$, RMSE = 3.0 h and a bias of 0.97 h (Figure 3f). This simplification increases the error but still appears useful in the Control cases.

As noted above, 'initial' values were taken at $t = 1.5$ h after landfall in the simulations because of the apparent early shock response. If we use values of $Rmax$ and $\tilde{P}$ taken at the moment of landfall ($t = 0$) with constant mean k and χ_0 as above this slightly increases the correlation of the model estimates with simulation half-lives ($R^2 = 0.74$) and increases the RMSE (3.06 h) and bias (2.08 h).

2) Model validation

The initial density-weighted column radial wind speed, $\mathcal{V}_r$, is shown as a function of radius, r, for the Control cases in Figure 4a. There is an approximately linear increase of $\mathcal{V}_r$ from the centre out to $Rmax_0$. Goodness-of-fit R^2 values for modelling $\mathcal{V}_r$ varying linearly with r during the decay are shown in Figure 4b. These remain high and in nearly all cases stay above 0.98 throughout the decay. That $\mathcal{V}_r$ varies linearly with r from $Rmax_0$ to near $r = 0$ throughout the decay means $\mathcal{V}_r$ at $Rmax_0$, χ, divided by $Rmax_0$ is an appropriate approximation of the radial gradient of $\mathcal{V}_r$ near the centre. This is an empirical validation of the assumption made in Equation 9.

The second assumption parameterises the core column speed as a function of pressure deficit. The parameter k was estimated by using least squares regression and Equation 12 for each decay case on values from $t = 1.5$ h to $t = 11.5$ hours after the imposition of land, with γ left as a free variable in the regression. The mean value of k was 1.30 in the Control cases with a standard deviation of 0.35. The mean goodness-of-fit parameter R^2 in the Control cases was 0.89 suggesting the assumption that the core column speed, χ, decays as $\tilde{P}^k$ holds reliably in the idealised decay experiments across a wide range of conditions. The values of k and R^2 for each case are listed in Table 1. χ as a function of $\tilde{P}$ with fitted decay curves are shown in Figure 4c.

Decay of $\tilde{P}$ as function of time in the numerical simulations and as predicted by Equation 15 when using values of k and χ_0 evaluated per experiment is shown in Figure 4d. The mean RMSE across the Control experiments was 0.0012. When a constant mean k is used the RMSE increases to 0.0020 (Figure 4e). Finally when using both constant mean k and χ_0 the mean RMSE increases to 0.0028 (Figure 4f).

c. Dry experiments

The Dry runs decayed at twice the rate with a mean half-life of 4.8 hours. The half-life for each decay case is shown in Table 1. The decay half-life is shown as a function of initial TC parameters in Figure 5 for the Dry cases. The half-life is strongly correlated with $Rmax_0$ with an R^2 value of 0.97 (p-values < 0.001). $\tilde{P}_0$ is not significantly correlated (at the 95% confidence level) with half-life ($R^2 = 0.12$, p-value = 0.25). Again, excluding case 2, which may appear to be an outlier (Figure 5b), results in $\tilde{P}_0$ becoming significantly anti-correlated (at the 95% confidence level) with half-life. As in the control cases, a large range of half-life values is observed with very similar values of $\tilde{P}_0$ for the sets of cases initialized during the slow decay of the spin-up TC (from day 7 onwards). χ_0 is moderately correlated with the half-life in the Dry cases ($R^2 = 0.54$).

1) Model performance

We use Equation 18 using k and χ_0 evaluated per experiment to calculate model estimate half-lives and compare these to the simulation half-lives in Figure 5d. The quantities are very highly correlated with $R^2 = 0.99$ and an RMSE of 0.75 h. The model half-life has a mean positive bias of 0.65 h. We then use a constant k equal to the mean value of k for the Dry experiments ($\overline{k} = 1.63$) and perform the same comparison (Figure 5e). Model estimated half-life is still very strongly correlated with simulation half-life with an R^2 value of 0.97. The RMSE is 0.68 h and the bias is at 0.61 h. We can again make the simplification of using a both a constant k and χ_0 (mean across cases) for the Dry experiments ($\overline{\chi_0} = -0.047$ m s^{-1}) which gives $R^2 = 0.93$, RMSE = 1.57 h and a bias of 0.81 h. This simplification work remarkably well for the Dry cases.

2) Model validation

As for the Control cases we present model validation analysis in Figure 6. The initial column radial wind speed, $\mathcal{V}_r$, is shown as a function of radius, r, in both the Control and Dry cases in Figure 6a. There is an approximately linear increase of $\mathcal{V}_r$ from the centre out to $Rmax_0$. Goodness-of-fit R^2 values for modelling $\mathcal{V}_r$ varying linearly with r during the decay remain high and in nearly all cases stay above 0.98.

The mean value of k was 1.63 with a standard deviation of 0.09. The mean goodness-of-fit parameter R^2 in the Dry cases and 0.99 suggesting the assumption that the core column speed, χ, decays as $\tilde{P}^k$ holds reliably in the idealised decay experiments across a wide range of conditions.

The values of k and R^2 for each case are listed in Table 1. χ as a function of $\tilde{P}$ with fitted decay curves are shown in Figure 6c.

Decay of $\tilde{P}$ as function of time in the numerical simulations and as predicted by Equation 15 when using values of k and χ_0 evaluated per experiment is shown in Figure 6d. The mean RMSE across the Control experiments was 0.0029. When a constant mean k is used the RMSE increases to 0.0030 (Figure 6e). Finally when using both constant mean k and χ_0 the mean RMSE increases to 0.0040 (Figure 6f).

d. Decay structure

We now examine the structure of the azimuthal average tangential wind speed, v_t, near the start of the decay and 10 hours into the decay for a control case (Figure 7a,b). We choose this case as a representative sample and find similar behaviour across all cases. In the Control case at t = 1 h we find a well defined maximum v_t at a height of approximately 1.5 km at approximately 20 km radius with speeds exceeding 90 m s^{-1}. By t = 10 h maximum speeds have reduced to around 40 m s^{-1} but there are three local maxima, one at the top of the inflow layer close to Rmax, and two broad mid-level maxima at approximately 20 and 80 km. Similar analysis of azimuthal average radial wind speed, v_r, shows that maximum boundary layer inflow speeds decay from over 40 m s^{-1} to 14 m s^{-1} over the period t = 1 to 10 hours (Figure 7c,d). At t = 1 hour a substantial outflow channel is apparent beginning at around 1 km near $Rmax$ and rising outwards to the upper levels. Maximum outflow speeds reach 28 m s^{-1}. By t = 10 h the maximum outflow speed has reduced to 5 m s^{-1}.

In the Dry case, the situation at t = 1 h is similar to the Control with a low-level maximum v_t albeit with attenuated speeds (Figure 8a). However by t = 10 h the picture is dramatically different, low-level speeds have largely been reduced to below 10 m s^{-1}. However, a broad mid-level wind speed maximum centred at a height of about 7 km and at a radius of 40 km has maintained with speeds above 50 m s^{-1} (Figure 8b). Analysis of v_r shows that at 1 h the maximum inflow speed is 26 m s^{-1}, and outflow speeds are below 10 m s^{-1}, substantially reduced compared to the Control case. By 10 h all radial wind speeds have reduced to only a few m s^{-1} even though a substantial vortex is still present in the mid-levels 8c,d).

The maximum wind speeds at a height 10 m and 7 km is shown as a function of time for the Control and Dry case 5 in Figure 9. The 10 m and 7 km maximum wind speeds decay at a similar rate in the Control case falling to around half their initial values by around $t = 10$ h. However in the Dry case the 7 km maximum wind speed decays at a much slower rate that the 10 m wind speed. The mid-level wind speeds is decoupled from the surface level wind speed. This phenomenon is apparent from immediately after the onset of decay until at least $t = 24$ h when the maximum wind speed is 44 m s^{-1} at 7 km but only 6 m s^{-1} at 10 m. In summary, the surface wind speed is coupled to the mid-level wind in the Control case but decoupled in the Dry case.

5. Discussion

a. Simulations

Our set of idealized land-induced decay numerical experiments cover a wide range of initial conditions with a range of $\Delta P_0/Rmax_0$ similar to those observations reported by Vickery (2005). The decay constants of the simulations also have a similar dependence on $\Delta P_0/Rmax_0$ as reported by Vickery (2005). This close match is perhaps surprising given the idealized nature of our experiments (instantaneous land, no translation, no shear) but gives confidence that our set of experiments does represent the range of TCs making landfall in nature and capture at least some of the important physical processes which determine the rates at which they then decay. Therefore the simulations are useful to validate the assumptions of the analytic model.

We find a strong dependence of simulated decay half-life of central pressure deficit on the initial radius of maximum wind speed, $Rmax_0$, in both the Control and Dry cases (Figures 3 and 5). This is especially clear in the Dry cases ($R^2 = 0.97$). In the more realistic Control cases the presence of convection fundamentally changes the decay process (see Section 1) leading to a noisier dependence of the half-life on $Rmax_0$ ($R^2 = 0.76$). This dependence of pressure deficit decay rate increasing inversely with the radius can be understood in terms of the dominant role of mass convergence during the decay.

Control and Dry decay experiments initialized during the early stage of the Spin-up TC (case no. < 7) have similar half-lives with very different $\tilde{P}_0$ whereas for cases initialized during the late stage of the Spin-up TC (case no. > 7) $\tilde{P}_0$ stays approximately constant while the half-life changes. In fact the effect of the variation in $\tilde{P}_0$ on the decay in the early stage cases is largely offset by a similar variation in χ_0, so variation in $Rmax_0$ dominates the changes in decay. In late stage experiments, when $\tilde{P}_0$ is approximately constant, the effect of an increasing $Rmax_0$ is tempered by an increasing χ_0. Overall this leads to the very strong correlation of $Rmax_0$ with the simulated half-life in our experiments. The relatively weak correlation between half-life and $\tilde{P}_0$ in our Control ($R^2 = 0.27$) and Dry ($R^2 = 0.12$) simulations is certainly related to the limited variability of $\tilde{P}$ after day seven of the Spin-up simulation. This is a property of our simulations rather than a fundamental relationship between $\tilde{P}_0$ and half-life.

While the analytic decay model predicts a linear dependence of half-life on the $Rmax$ and $\tilde{P}_0$ and an inverse dependence on χ_0, most of the 'skill' in the half-life prediction in our sets of simulations comes from the variability of $Rmax_0$ (see correlations of half-life with $Rmax_0$, $\tilde{P}_0$ and χ_0 in Figure 3). This can be partly explained through analysis of the coefficient of variation (CV) of the parameters. The CV of $Rmax_0$ is approximately double that of both $\tilde{P}_0$ and χ_0 in both the Control and Dry cases. Note this is not necessarily reflective of the statistics of real world landfalling TCs. Furthermore, $Rmax_0$ and χ_0 are not significantly correlated in the Control experiments ($R^2 = 0.15, p = 0.18$) and have very different relationships with half-life. This supports our choice to parameterise the radial gradient of column-integrated radial wind speed, $\frac{\mathrm{d}\mathcal{V}}{\mathrm{d}r}$, in terms of $Rmax_0$ and χ in Equation 9 allowing $Rmax_0$ and χ_0 to be treated as independent variables controlling the rate of pressure filling and ultimately the half-life of the decay.

The large vertical variability of the radial flow makes $\mathcal{V}_r$ very difficult to directly observe for real cases, and k is not directly observable and here is estimated from the decay simulation data. Hence estimating the decay half-life using the model requires knowledge of quantities not observable at the time of landfall. It is worth noting however that the model can still produce useful estimates of decay half-life even if constant estimates of k and χ_0 are used. The model with $\chi_0 = 0.026$ m s^{-1} and $k = 1.30$ may therefore be a practical zero-order estimate of real decay half-lives without knowledge of χ_0 and k. This half-life equation then depends only on the observable initial size and pressure deficit:

$$\hat{t}_{1/2} \approx 4\tilde{P}_0 Rmax_0 \tag{20}$$

where $\hat{t}_{1/2}$ is the half-life in hours, $\tilde{P}_0$ is the initial central pressure deficit fraction and $Rmax_0$ is the initial radius of maximum surface wind speed in km and the dimensions of χ have been absorbed into the constant giving it units of h km^{-1}. This is the simplest form of the decay within our framework.

1) Role of moisture

We found that on average the Dry experiments half-life (4.8 h) decayed at approximately twice the rate of the Control experiments (10.5 h). Figure 8 shows that in a Dry case, a strong mid-level vortex persists after 10 h by which time surface friction has destroyed boundary layer wind speeds. The boundary layer has become decoupled from the vortex above it and the frictional braking effects from the surface roughness are felt only within this shallow layer. However in the Control case 5 the boundary layer is still coupled to the layer above with similar wind speeds seen in both after 10 h. The Dry decoupling results from the lack of convection and much reduced secondary circulation. The Control case transmits the frictional braking felt in the boundary layer into the vortex above though the vertical ascent of lower angular momentum. Thus the height of the vortex experiencing frictional braking is much larger in the Control case. Indeed, we can use the spin down half-life formula proposed by Eliassen and Lystad (1977) and Phillipson and Toumi (2021) to infer vortex height of 5.0 km for the Dry and 12.1 km in the Control cases.

b. Analytic model

The new analytic physically based framework allows estimates of decay half-life using three TC initial state parameters and a fitted parameter k. It differs from other decay models in that it starts with considerations of mass flux and pressure rather than making only empirical assumptions. The model shows that the initial size of the inner core, represented as $Rmax$, is a key parameter controlling the rate of land-induced decay, with the rate of decay inversely proportional to size. The choice of $Rmax$ itself is somewhat arbitrary and any quantity reflecting the spatial scale of the inner core would give similar results. $Rmax$ was chosen as it is a well-known, frequently used TC parameter and has been recorded for decades in historical TC databases. The linear dependence of the decay rate on $Rmax$ predicted by the model offers a theoretical explanation for the empirical result of Vickery (2005) who found the same linear dependence in the historical record of Atlantic hurricanes. Following Malkin (1959) and DeMaria et al. (2006) they suggest that "smaller storms would tend to decay more rapidly than larger storms since a relatively larger portion of the core of the storm is removed from the energy source more rapidly than in the case of a larger storm". Our simulations confirm the observations, but our model shows that the decay rate is a more fundamental property of the TC vortex geometry and that for the same initial central pressure deficit and core column speed, a large storm will decay slower than a smaller storm.

Existing theoretical wind speed decay models for TCs are framed in terms of the frictional interaction of the land surface with the TC, and how this leads to a reduction in surface wind speed over time. A theoretical model for turbulent surface drag driven spin-down of cyclones (Eliassen 1971; Eliassen and Lystad 1977) is also successful in predicting the decay rate of hurricane strength $Vmax$ over the ocean (Montgomery et al. 2001) and land (Phillipson and Toumi 2021). That model predicts an algebraic form for the decay of angular momentum (or tangential speed) and a half-life which is proportional to the vortex height and inversely proportional to the drag coefficient, C_D, and the initial tangential speed. There is no explicit dependence of $Vmax$ decay on size and this appears fundamentally different to our pressure model. Our model considers the mass in the column and the Eliassen model aims to explain the boundary layer wind at the surface.

The surface pressure model also introduces a new concept, the core column speed, χ - a radial wind speed representative of the whole column at $Rmax_0$. The column theoretically captures all mass fluxes which make significant contributions to surface pressure tendency. We note that as shown in Figure 1 the core size as measured by $Rmax$ tends to shrink during the first hours of the land-induced decay experiments. While this phenomenon is interesting in its own right and may prove important in a developing a full understanding of post-landfall dynamics, it is not directly relevant to the decay model we present because χ is defined at the initial radius of maximum winds. We only require that the linearity assumption made in Equation 9 remains valid out to $Rmax_0$ throughout the decay process we are modelling.

χ_0 is clearly a simplification of the many factors that affect radial flow at all heights. In practice χ_0 is a small residual of the difference between the large outflow speeds at upper levels and large inflow speeds and will therefore depend on many physical processes governing inflow and outflow during the decay. Partly because of this difference of large numbers, the initial core column speed is not easily observable and even calculating it from instantaneous simulation output is challenging. This means that at present we could not evaluate $\hat{t}_{1/2}$ directly given standard real-world TC metrics. However, given that we expect it to be governed by a combination of near-surface inflow related physics and upper level outflow related physics it maybe possible to parameterise χ_0 in terms of other, more readily available physical quantities. For example, we observe that χ_0 is dependent on the TC moisture through latent heating. In the Dry experiments, where convective heating is suppressed, the initial core column speed is almost double that in the Control cases. Finally, even just assuming a constant χ_0 value still enables useful predictions of the half-life.

Equation 8 shows that the central pressure tendency is proportional to the central pressure. This leads to the result that the decay half-life is proportional to the initial pressure deficit (Equation 18). That is, for a given initial radius of maximum wind speed and core column speed, TCs with a larger central pressure deficit, therefore smaller central pressure, decay more slowly. Larger pressure deficits take more time to fill and this makes intuitive sense. We can only expect to see this relationship in observations of landfalling TCs if we control for initial radius of maximum wind speed and core column speed (not observed). Even in our own small set of landfall simulations initial central pressure deficit is weakly anti-correlated with half-life. In observational studies Vickery and Twisdale (1995) and Vickery (2005) report that the decay rate increases with initial central pressure deficit. However, these studies did not clearly separate out the simultaneous effect of size. At least some of the strongest storms could also be small. We note that the simulations (and thus our model) agree with the observations of the decay constants as function of the ratio of the pressure deficit and radius reported by Vickery (2005) (see Figure 2). Kaplan and Demaria (1995) show that storms with stronger surface winds ($Vmax$) decay more rapidly in agreement with the decay models of Phillipson and Toumi (2021) and Chen and Chavas (2021). Neither of these studies account for the effect of TC size. Furthermore, the decay in surface winds and surface pressure are at least partially decoupled, hence traditional wind-pressure relationships are not applicable during landfall decay. We may therefore expect decay rates of surface wind ($Vmax$) and pressure deficit to have different controlling factors.

1) Model assumptions

The derivation of our decay model makes two main assumptions. The first is that the column speed varies linearly with radius (Equation 9) from the centre to $Rmax_0$. This assumption appears justified by the results of the simulations. High R^2 values throughout the decay in the Control and the Dry cases show that χ and r are highly linear throughout the decay within the core. This suggests the assumption is robust as the cases cover a wide range of initial conditions and decay environments. However, the assumption does not hold during the initial shock response caused by our simulation experimental design, with large non-linear fluctuations near the centre (not shown).

The second assumption, that χ decays as $\tilde{P}^k$ (Equation 12), also seems well-founded. In the Control experiments the mean k parameter was 1.30, reasonably close to 1, at which the decay of central pressure deficit would appear exponential. Vickery (2005) amongst others assume exponential decays in the historical record of landfalling TCs. The mean k in the Dry cases was significantly higher at 1.63. This difference in k only leads to a 15% increase in β from 0.77 to 0.87 from the Control to the Dry simulations due to the form of Equation 19. This change actually acts to increase the estimated half-life by 13%. The large reduction in half-lives in the Dry simulations is due to much larger χ_0 acting in opposition to the slightly larger values of k.

A larger k in the Dry case reflects the faster radial inflow reduction for a similar pressure deficit reduction during the decay compared to the Control decay. In the Dry case almost all the filling happens in the boundary layer and this column speed is rapidly diminished as the inflow collapses. However, the estimated half-life is relatively insensitive to k. We find using a mean value of k for each of the Control and Dry experiment sets can be sufficient to predict the half-life (as in Figures 3d and 5d).

The approximation made in obtaining Equation 14 depends on the central pressure deficit fraction being small ($\tilde{P} \ll 1$). Fractional errors in the central pressure deficit fraction tendency due to this approximation are equal to the central pressure deficit fraction itself. In our simulations $\tilde{P}$ is usually below 0.1 so we expect errors in the tendency due to this approximation to be less than 10% and for the half-life less than that.

2) Wider implications

It is plausible that this pressure filling framework has wider applications as a zero order model. The decay of tropical cyclones over the ocean can also be considered in this framework. The detailed physical causes may be lower sea surface temperatures, wind shear and/or interactions with mid-latitude weather. In the model the effect of these physical causes is ultimately captured and collapsed into the column speed. Similarly, in the case of extra-tropical cyclones we suspect the model is also applicable. The physical cause of the column speed may vary but the half-life linear dependence on initial pressure deficit and size (due to the critical role of convergence) should be robust as they are derived from mass continuity. More research is required to confirm this.

Here we find that the pressure filling half-life depends on the TC state itself, in particular the initial pressure and size. There will therefore be a strong dependence on initial conditions, the state of the TC at the time of landfall. This is quite different from a simple exponential decay where the time constant would just be dependent on environmental conditions and independent of the initial condition. It is not sufficient for forecasts just to know just the environmental conditions, which will affect, for example, the column speed. The strong dependence of the actual time evolution on the initial TC conditions makes it clear that forecasting land decay is very challenging.

Given the limitations of the set of experiments examined here (idealized, limited sampling of initial states) a natural extension to this work would be to test the performance of this new model on a comprehensive set of realistic numerical simulations of landfalling TCs.

6. Conclusion

We propose a simple physically based analytical model of pressure filling after landfall and test it against simulations. The simulated half-life of the TC pressure deficit decay increases with TC size in a set of idealized land numerical simulations. When these simulations are simplified, by removing all moisture and therefore latent heating, the decay rate is doubled and the dependence on the size is made even clearer. Despite its simplifications the analytic model does give useful insight. A fundamental insight is that the central pressure deficit half-life is proportional to the initial core size. The initial pressure deficit and the initial core column speed are also important. This framework is quite different from a simple exponential decay.

Acknowledgments. This work was supported by the Natural Environment Research Council/UKRI (NE/V017756/1) and the UK-China Research and Innovation Partnership Fund through the Met Office Climate Science for Service Partnership (CSSP) China as part of the Newton Fund.

Data availability statement. Numerical simulation data are available from the authors upon request.

References

Batts, M., E. Simiu, and L. Russell, 1980: Hurricane Wind Speeds in the United States. *Journal of the Structural Division*, **106**, 2001–2016.

Chen, J., and D. R. Chavas, 2020: The Transient Responses of an Axisymmetric Tropical Cyclone to Instantaneous Surface Roughening and Drying. *Journal of the Atmospheric Sciences*, **77 (8)**, 2807–2834, doi:10.1175/JAS-D-19-0320.1, URL https://doi.org/10.1175/JAS-D-19-.

Chen, J., and D. R. Chavas, 2021: Can existing theory predict the response of tropical cyclone intensity to idealized landfall? *Journal of the Atmospheric Sciences*, **78 (10)**, 3281–3296, doi:10.1175/JAS-D-21-0037.1, URL https://journals.ametsoc.org/view/journals/atsc/78/10/JAS-D-21-0037.1.xml.

DeMaria, M., J. A. Knaff, and J. Kaplan, 2006: On the decay of tropical cyclone winds crossing narrow landmasses. *Journal of Applied Meteorology and Climatology*, **45 (3)**, 491–499, doi:10.1175/JAM2351.1, URL http://journals.ametsoc.org/jamc/article-pdf/45/3/491/3532952/jam2351_1.pdf.

Eliassen, A., 1971: On the Ekman Layer in a circular Vortex. *Journal of the Meteorological Society of Japan. Ser. II*, **49A (0)**, 784–789, doi:10.2151/jmsj1965.49a.0{_}784, URL https://www.jstage.jst.go.jp/article/jmsj1965/49A/0/49A_784/_article.

Eliassen, A., and M. Lystad, 1977: The Ekman layer of a circular vortex. A numerical and theoretical study. Universitetsforlaget, URL https://ui.adsabs.harvard.edu/abs/1977GeoNr..31....1E/abstract, 1–16 pp.

Friedl, M. A., D. Sulla-Menashe, B. Tan, A. Schneider, N. Ramankutty, A. Sibley, and X. Huang, 2010: MODIS Collection 5 global land cover: Algorithm refinements and characterization of new datasets. *Remote Sensing of Environment*, **114 (1)**, 168–182, doi:10.1016/j.rse.2009.08.016.

Hlywiak, J., and D. S. Nolan, 2021: The Response of the Near-Surface Tropical Cyclone Wind Field to Inland Surface Roughness Length and Soil Moisture Content during and after Landfall. *Journal of the Atmospheric Sciences*, **78 (3)**, 983–1000, doi:10.1175/JAS-D-20-0211.1, URL www.ametsoc.org/PUBSReuseLicenses.

Ho, F. P., J. C. Su, K. L. Hanevich, R. J. Smith, and F. P. Richards, 1987: Hurricane climatology for the Atlantic and Gulf coasts of the United States. *NOAA Technical Report NWS*, **38**, URL https://repository.library.noaa.gov/view/noaa/7136.

Hong, S., and J. Lim, 2006: The WRF single-moment 6-class microphysics scheme (WSM6). *Journal of the Korean Meteorological Society*, **42 (2)**, 129–151, URL http://www.mmm.ucar.edu/wrf/users/docs/WSM6-hong_and_lim_JKMS.pdf%5Cnhttp://search.koreanstudies.net/journal/thesis_name.asp?tname=kiss2002&key=2525908.

Iacono, M. J., J. S. Delamere, E. J. Mlawer, M. W. Shephard, S. a. Clough, and W. D. Collins, 2008: Radiative forcing by long-lived greenhouse gases: Calculations with the AER radiative transfer models. *Journal of Geophysical Research*, **113 (D13)**, D13 103, doi:10.1029/2008JD009944, URL http://doi.wiley.com/10.1029/2008JD009944.

Janjic, Z., 1994: The step-mountain eta coordinate model: Further developments of the convection, viscous sublayer, and turbulence closure schemes. *Monthly Weather Review*, **122**, 927–945, URL http://journals.ametsoc.org/doi/abs/10.1175/1520-0493(1994)122%3C0927:TSMECM%3E2.0.CO;2http://journals.ametsoc.org/doi/abs/10.1175/1520-0493(1994)122%3C0927:TSMECM%3E2.0.CO%3B2.

Janjic, Z., 2002: Nonsingular Implementation of the Mellor-Yamada Level 2.5 Scheme in the NCEP Meso model. *NCEP Office Note*, **437**, 61, URL http://www.emc.ncep.noaa.gov/officenotes/newernotes/on437.pdf.

Jarvinen, B. R., A. B. Damiano, and G. J. D. Lockett, 1985: A storm surge atlas for Corpus Christi, Texas. *NOAA Technical Memorandum NWS NHC*, **27**, URL https://repository.library.noaa.gov/view/noaa/7187.

Jordan, C. L., 1958: Mean Soundings for the West Indies Area. *Journal of Meteorology*, **15 (1)**, 91–97, doi:10.1175/1520-0469(1958)015<0091:MSFTWI>2.0.CO;2, URL http://journals.ametsoc.org/doi/abs/10.1175/1520-0469%281958%29015%3C0091%3AMSFTWI%3E2.0.CO%3B2.

Kaplan, J., and M. Demaria, 1995: A simple empirical model for predicting the decay of tropical cyclone winds after landfall. *Journal of Applied Meteorology*, **34 (11)**, 2499–2512, doi:10.1175/1520-0450(1995)034<2499:ASEMFP>2.0.CO;2, URL http://journals.ametsoc.org/jamc/article-pdf/34/11/2499/3896649/1520-0450.

Li, L., and P. Chakraborty, 2020: Slower decay of landfalling hurricanes in a warming world. *Nature*, **587 (7833)**, 230–234, doi:10.1038/s41586-020-2867-7, URL https://doi.org/10.1038/s41586-020-2867-7.

Malkin, W., 1959: Filling and intensity changes in hurricanes over land. Tech. rep., U.S. Weather Bureau, Washington, DC, 18 pp.

Montgomery, M. T., H. D. Snell, and Z. Yang, 2001: Axisymmetric spindown dynamics of hurricane-like vortices. *Journal of the Atmospheric Sciences*, **58 (5)**, 421–435, doi:10.

1175/1520-0469(2001)058<0421:ASDOHL>2.0.CO;2, URL http://journals.ametsoc.org/jas/article-pdf/58/5/421/3458098/1520-0469.

Phillipson, L. M., and R. Toumi, 2021: A Physical Interpretation of Recent Tropical Cyclone Post-Landfall Decay. *Geophysical Research Letters*, **48 (18)**, e2021GL094 105, doi:10.1029/2021GL094105, URL https://onlinelibrary.wiley.com/doi/full/10.1029/2021GL094105https://onlinelibrary.wiley.com/doi/abs/10.1029/2021GL094105https://agupubs.onlinelibrary.wiley.com/doi/10.1029/2021GL094105.

Skamarock, W. C., and Coauthors, 2019: A Description of the Advanced Research WRF Version 4. *NCAR Tech. Note NCAR/TN-556+STR*, 145.

Vickery, P. J., 2005: Simple empirical models for estimating the increase in the central pressure of tropical cyclones after landfall along the coastline of the United States. *Journal of Applied Meteorology*, **44 (12)**, 1807–1826, doi:10.1175/JAM2310.1, URL http://journals.ametsoc.org/jamc/article-pdf/44/12/1807/3295013/jam2310_1.pdf.

Vickery, P. J., and L. A. Twisdale, 1995: Wind-Field and Filling Models for Hurricane Wind-Speed Predictions. *Journal of Structural Engineering*, **121 (11)**, 1700–1709, doi:10.1061/(asce)0733-9445(1995)121:11(1700), URL https://ascelibrary.org/doi/abs/10.1061/%28ASCE%290733-9445%281995%29121%3A11%281700%29.

Wang, S., and R. Toumi, 2016: On the relationship between hurricane cost and the integrated wind profile. *Environmental Research Letters*, **11 (11)**, 114 005, doi:10.1088/1748-9326/11/11/114005, URL http://stacks.iop.org/1748-9326/11/i=11/a=114005?key=crossref.b8c4fd8906504a99c87f1218d5c8042f.

Wang, S., and R. Toumi, 2019: Impact of Dry Midlevel Air on the Tropical Cyclone Outer Circulation. *Journal of the Atmospheric Sciences*, **76 (6)**, 1809–1826, doi:10.1175/jas-d-18-0302.1, URL http://journals.ametsoc.org/doi/10.1175/JAS-D-18-0302.1.

LIST OF TABLES

Table 1. Exp is the experiments type: Control is normal, Dry is with all moisture removed from the atmosphere. t_{lf} is the time in days after the initialisation of the Spin-up run at which the land experiment began. $Vmax$ is the maximum wind speed at 10 m in m s^{-1}, $Rmax$ is the radius of maximum wind speed at 10 m in km, $\tilde{P}$ is the central pressure deficit fraction, χ is the column radial wind speed in m s^{-1} with subscript lf denoting value at time land is imposed in simulation ($t = 0$ h) and subscript 0 denoting 'initial' values used in model taken at $t = 1.5$ h. k is the estimated decay exponent (Equation 12) and R_k^2 is the quality of fit parameter for the estimation of k. $t_{1/2}$ is the simulation half-life of the pressure deficit. $\hat{t}_{1/2}$ is the model half-life estimated by Equation 18. $\hat{t}_{1/2,\overline{k}}$ is model half-life with constant mean k. $\hat{t}_{1/2,\overline{k},\overline{\chi}}$ is model half-life with constant mean k and χ_0. 35

TABLE 1. Exp is the experiments type: Control is normal, Dry is with all moisture removed from the atmosphere. t_{lf} is the time in days after the initialisation of the Spin-up run at which the land experiment began. $Vmax$ is the maximum wind speed at 10 m in m s^{-1}, $Rmax$ is the radius of maximum wind speed at 10 m in km, $\tilde{P}$ is the central pressure deficit fraction, χ is the column radial wind speed in m s^{-1} with subscript lf denoting value at time land is imposed in simulation ($t = 0$ h) and subscript 0 denoting 'initial' values used in model taken at $t = 1.5$ h. k is the estimated decay exponent (Equation 12) and R_k^2 is the quality of fit parameter for the estimation of k. $t_{1/2}$ is the simulation half-life of the pressure deficit. $\hat{t}_{1/2}$ is the model half-life estimated by Equation 18. $\hat{t}_{1/2,\overline{k}}$ is model half-life with constant mean k. $\hat{t}_{1/2,\overline{k},\overline{\chi}}$ is model half-life with constant mean k and χ_0.

Exp	t_{lf}	$Vmax_{lf}$	$Vmax_0$	$Rmax_{lf}$	$Rmax_0$	$\tilde{P}_{lf}$	$\tilde{P}_0$	χ_0	k	R_k^2	$t_{1/2}$	$\hat{t}_{1/2}$	$\hat{t}_{1/2,\overline{k}}$	$\hat{t}_{1/2,\overline{k},\overline{\chi}}$
Control	2	40.4	35.5	26.7	24.7	0.050	0.048	0.0155	1.51	0.972	7.73	8.76	8.11	4.82
Control	3	51.9	43.3	24.0	24.0	0.080	0.069	0.0227	1.62	0.930	7.99	8.85	7.87	6.83
Control	4	68.4	59.4	20.0	18.7	0.115	0.101	0.0357	1.74	0.965	6.82	6.62	5.63	7.69
Control	5	65.4	57.5	21.3	19.3	0.113	0.101	0.0311	1.62	0.952	7.64	7.52	6.70	7.97
Control	6	57.1	49.9	26.7	24.7	0.094	0.086	0.0212	0.79	0.920	8.27	8.94	10.68	8.66
Control	7	45.7	38.4	37.3	28.7	0.071	0.068	0.0188	1.10	0.793	10.07	10.29	11.07	7.96
Control	8	46.9	38.9	42.7	38.0	0.071	0.066	0.0190	0.88	0.800	11.82	12.24	14.21	10.34
Control	9	47.5	40.0	42.7	44.0	0.075	0.070	0.0275	1.42	0.883	11.89	12.55	12.02	12.64
Control	10	45.6	37.7	49.3	49.3	0.071	0.067	0.0239	1.01	0.821	12.93	13.25	14.69	13.45
Control	11	44.0	35.4	54.7	55.3	0.071	0.065	0.0315	1.93	0.894	13.66	15.53	12.30	14.84
Control	12	45.2	37.5	60.0	62.0	0.073	0.068	0.0306	1.16	0.927	13.22	13.98	14.70	17.19
Control	13	42.4	35.3	65.3	72.0	0.069	0.067	0.0337	0.99	0.886	11.65	13.77	15.35	19.78
Control	14	40.4	31.3	68.0	71.3	0.064	0.060	0.0287	1.16	0.808	13.36	15.10	15.92	17.46
Dry	2	40.4	28.5	26.7	17.3	0.050	0.047	0.0218	1.47	0.982	3.58	4.21	4.47	2.09
Dry	3	51.9	37.9	24.0	17.3	0.080	0.067	0.0356	1.60	0.995	3.63	3.88	3.93	2.99
Dry	4	68.4	50.5	20.0	14.7	0.115	0.094	0.0480	1.59	0.999	3.41	3.40	3.45	3.55
Dry	5	65.4	48.7	21.3	16.0	0.113	0.093	0.0490	1.57	0.998	3.50	3.60	3.68	3.86
Dry	6	57.1	42.4	26.7	18.7	0.094	0.081	0.0429	1.50	0.998	3.79	4.05	4.25	3.91
Dry	7	45.7	33.1	37.3	24.0	0.071	0.065	0.0375	1.63	0.991	4.40	5.00	5.00	4.02
Dry	8	46.9	34.0	42.7	29.3	0.071	0.065	0.0415	1.61	0.988	4.78	5.51	5.55	4.93
Dry	9	47.5	34.4	42.7	32.7	0.075	0.070	0.0473	1.65	0.985	5.31	5.91	5.87	5.95
Dry	10	45.6	32.0	49.3	40.0	0.071	0.067	0.0491	1.69	0.990	5.68	6.70	6.56	6.91
Dry	11	44.0	31.6	54.7	46.0	0.071	0.068	0.0555	1.81	0.996	6.11	7.25	6.77	8.06
Dry	12	45.2	32.8	60.0	50.0	0.073	0.070	0.0603	1.70	0.994	6.11	7.15	6.98	9.03
Dry	13	42.4	30.9	65.3	51.3	0.069	0.067	0.0611	1.76	0.982	6.25	7.17	6.84	8.96
Dry	14	40.4	28.1	68.0	56.0	0.064	0.063	0.0568	1.63	0.974	6.35	7.47	7.48	9.10

LIST OF FIGURES

Fig. 1. Overview of numerical simulation experiments showing central pressure deficit fraction $\tilde{P}$, maximum azimuthal average 10 m wind speeds, $Vmax$, and radius of $Vmax$, $Rmax$, as a function of time. Spin-up simulation in blue, Land-induced decay experiments and Dry land-induced decay experiments in orange, and green respectively. 37

Fig. 2. Central pressure deficit exponential decay coefficient, $a = \frac{\ln 2}{\text{half-life}}$, against initial central pressure deficit, ΔP_0 divided by initial radius of maximum wind speed, $Rmax_0$, for the decay experiments (case numbers in red). Solid line is linear fit to our experiments (R^2 = 0.76). Dashed line is fit from Vickery (2005) Gulf Coast and Florida Peninsula region, dotted line is all regions. 38

Fig. 3. Simulated TC half-life of the Control cases against: (a) initial $Rmax$, (b) initial $\tilde{P}$, (c) initial χ, and (d, e, f) model estimated half-lives with subscripts $\overline{k}$ and $\overline{\chi}$ indicating use of constant mean values of $\overline{k} = 1.30$ and $\overline{\chi_0} = -0.026$ effectively. Model estimated half-lives evaluated using Equation 18. 39

Fig. 4. The density-weighted column mean radial wind speed, $\mathcal{V}_r$, as function of radius, r, at $t = 1.5$ h from the TC centre to the radius of maximum wind speed (a). Goodness-of-fit, R^2, of $\mathcal{V}_r$ as a linear function of r as a function of time (b). Decay of simulated TC column radial wind speed at radius of maximum wind speed, χ, as a function of $\tilde{P}$, with power law fit (Equation 12) (c). Mean k and goodness-of-fit parameter, R^2, shown. $\tilde{P}$ as a function of time with model prediction from Equation 15, with mean RMSE across the simulations (d), with constant mean k (e), and with both constant mean k and χ_0 (f). 40

Fig. 5. As in Figure 3 but for the Dry cases with $\overline{k} = 1.63$ and $\overline{\chi_0} = -0.047$ m s^{-1}. 41

Fig. 6. As in Figure 4 but for the Dry experiments. 42

Fig. 7. Azimuthally averaged tangential wind speed, v_t and radial wind speed v_r, as a function of radius, r, and height, z, for the Control case 5 (a, c) 1 hour and (b, d) 10 hours after simulated landfall. Dotted lines are 0 contours, dashed contours show intervals of 20 m s^{-1}. 43

Fig. 8. As in Figure 7 but for the Dry case 5. 44

Fig. 9. Maximum wind speed, $Vmax$, as a function of time after simulated landfall at heights 10 m and 7 km for the Control and Dry case 5. 45

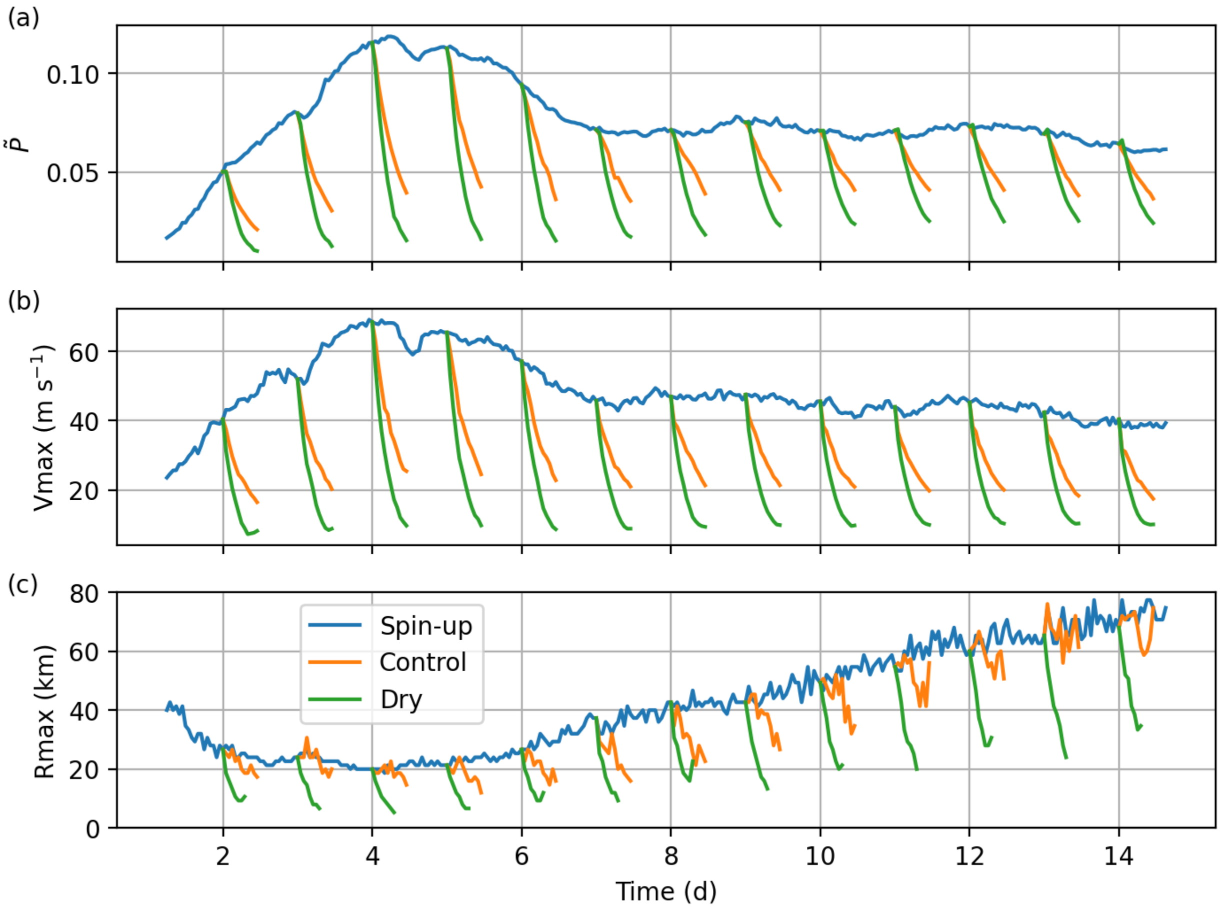

700 Fig. 1. Overview of numerical simulation experiments showing central pressure deficit fraction $\tilde{P}$, maximum
701 azimuthal average 10 m wind speeds, $Vmax$, and radius of $Vmax$, $Rmax$, as a function of time. Spin-up
702 simulation in blue, Land-induced decay experiments and Dry land-induced decay experiments in orange, and
703 green respectively.

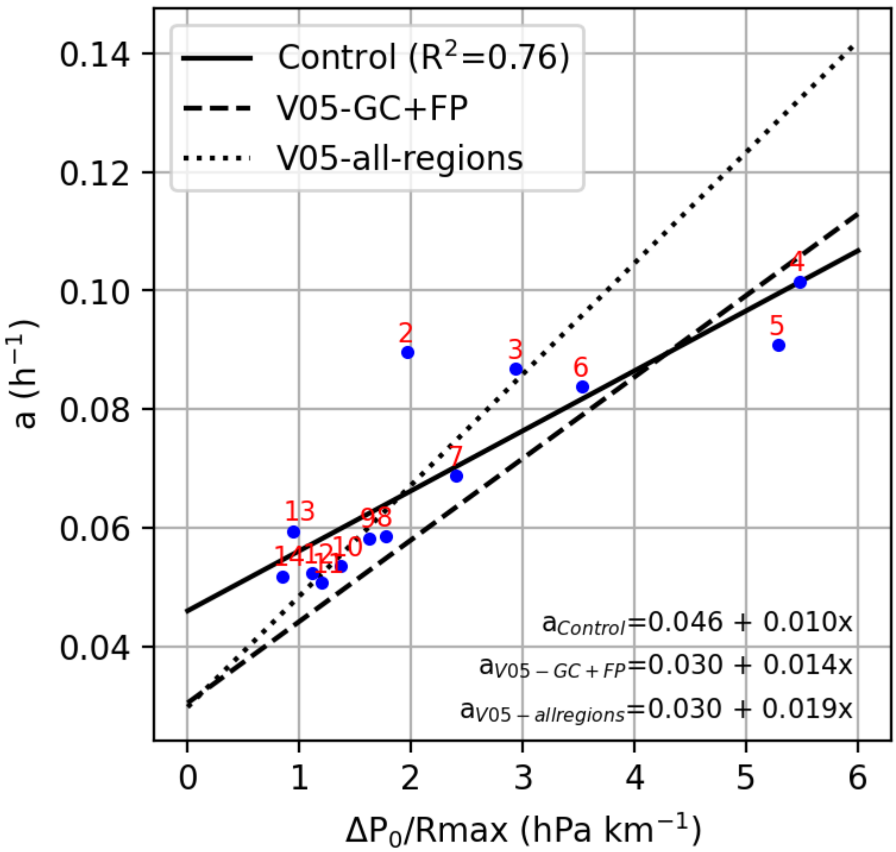

FIG. 2. Central pressure deficit exponential decay coefficient, $a = \frac{\ln 2}{\mathrm{half-life}}$, against initial central pressure deficit, ΔP_0 divided by initial radius of maximum wind speed, $Rmax_0$, for the decay experiments (case numbers in red). Solid line is linear fit to our experiments (R^2 = 0.76). Dashed line is fit from Vickery (2005) Gulf Coast and Florida Peninsula region, dotted line is all regions.

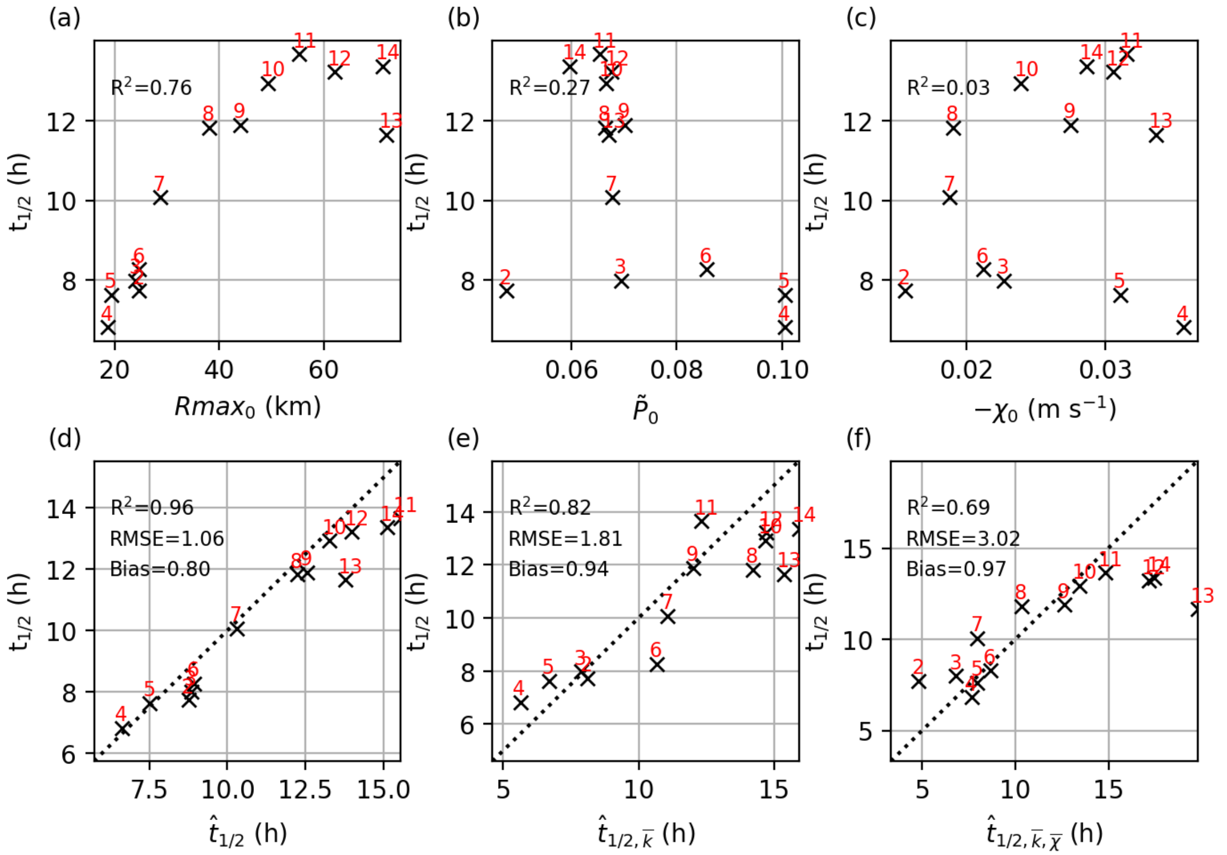

Fig. 3. Simulated TC half-life of the Control cases against: (a) initial $Rmax$, (b) initial $\tilde{P}$, (c) initial χ, and (d, e, f) model estimated half-lives with subscripts $\overline{k}$ and $\overline{\chi}$ indicating use of constant mean values of $\overline{k} = 1.30$ and $\overline{\chi_0} = -0.026$ effectively. Model estimated half-lives evaluated using Equation 18.

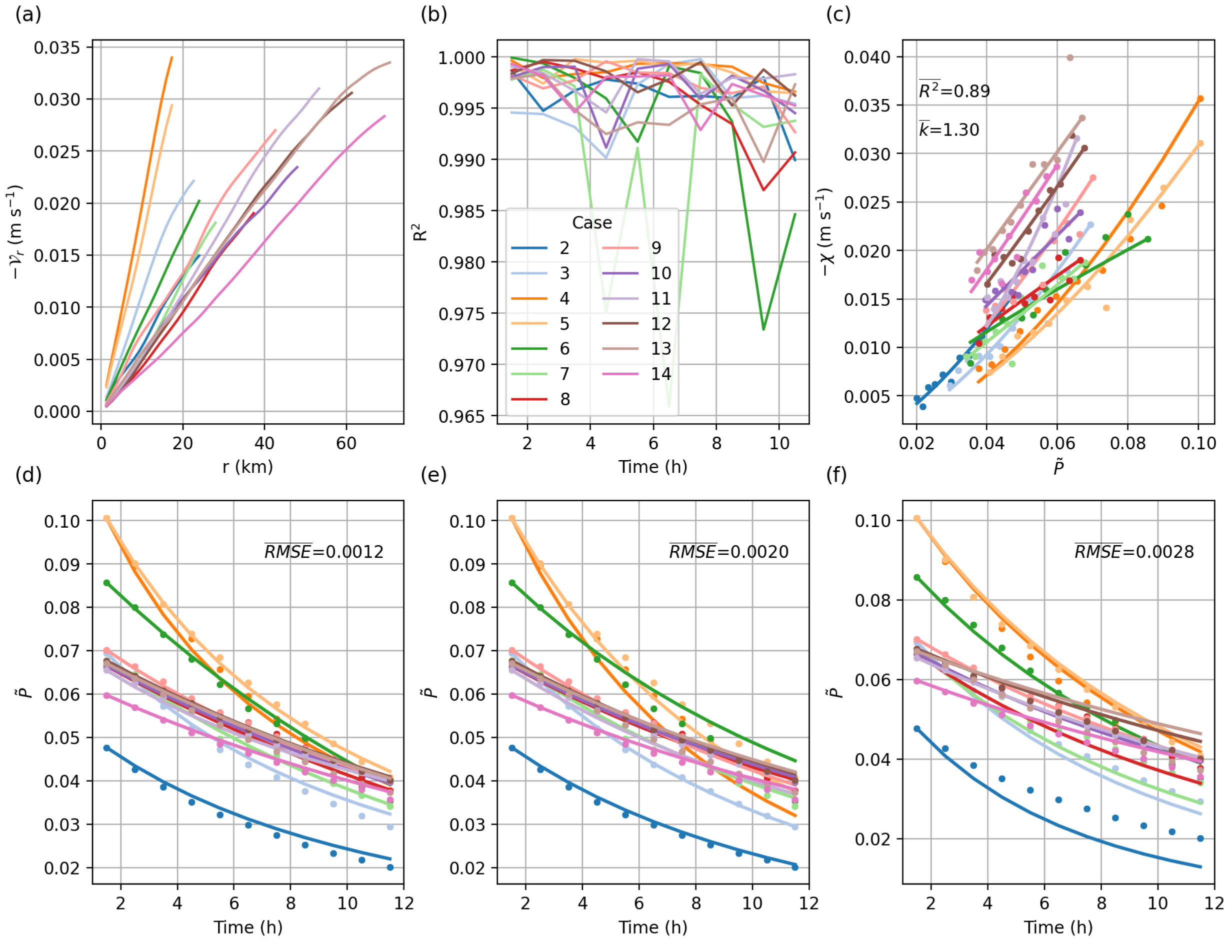

711 FIG. 4. The density-weighted column mean radial wind speed, $\mathcal{V}_r$, as function of radius, r, at $t = 1.5$ h from the TC centre to the radius of maximum wind speed (a). Goodness-of-fit, R^2, of $\mathcal{V}_r$ as a linear function of r as a function of time (b). Decay of simulated TC column radial wind speed at radius of maximum wind speed, χ, as a function of $\tilde{P}$, with power law fit (Equation 12) (c). Mean k and goodness-of-fit parameter, R^2, shown. $\tilde{P}$ as a function of time with model prediction from Equation 15, with mean RMSE across the simulations (d), with constant mean k (e), and with both constant mean k and χ_0 (f).

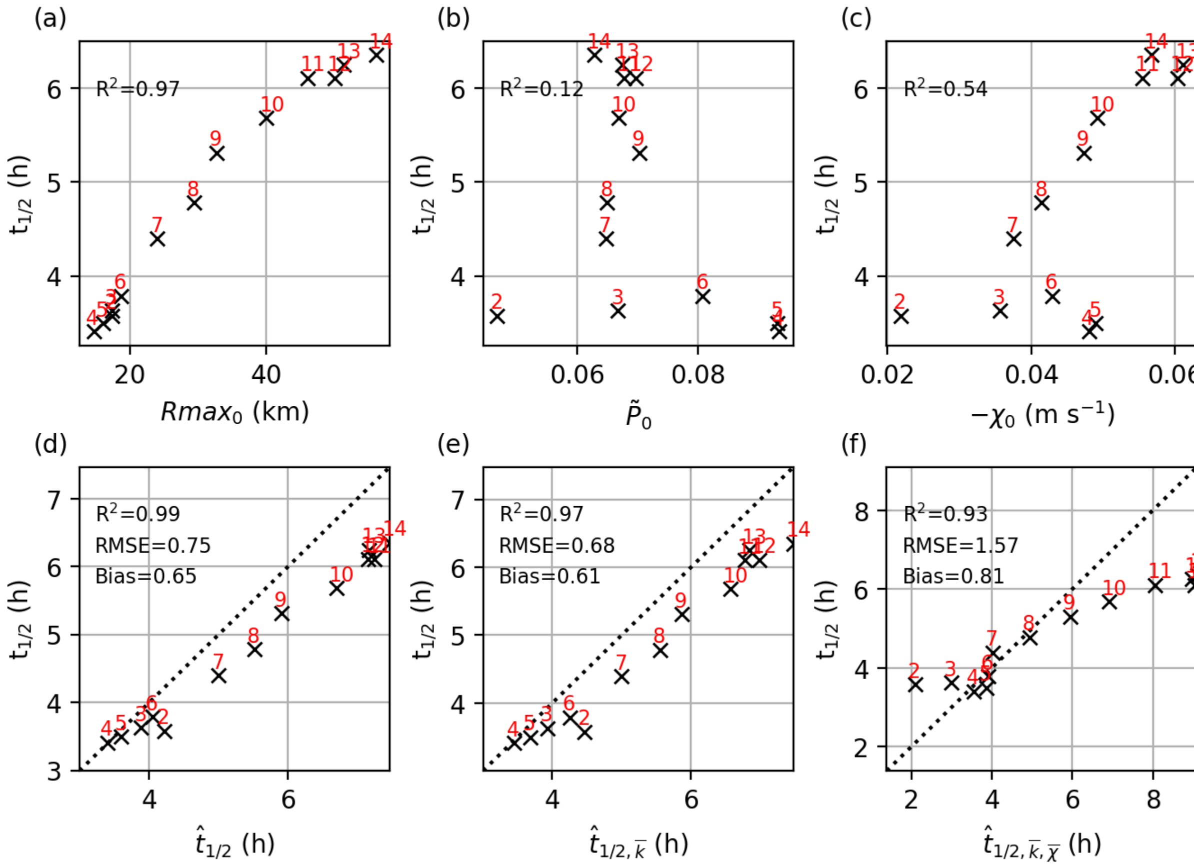

Fig. 5. As in Figure 3 but for the Dry cases with $\overline{k} = 1.63$ and $\overline{\chi_0} = -0.047$ m s^{-1}.

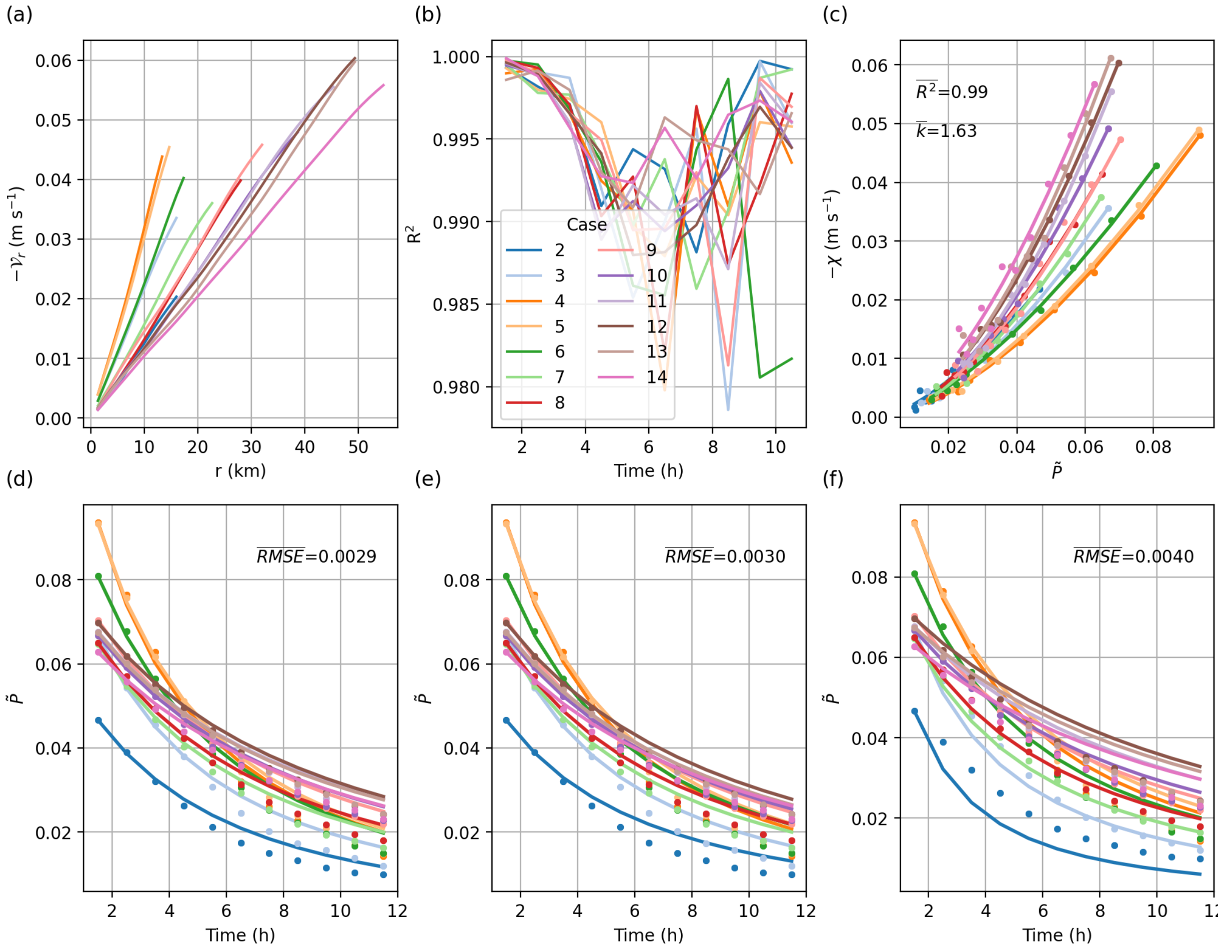

FIG. 6. As in Figure 4 but for the Dry experiments.

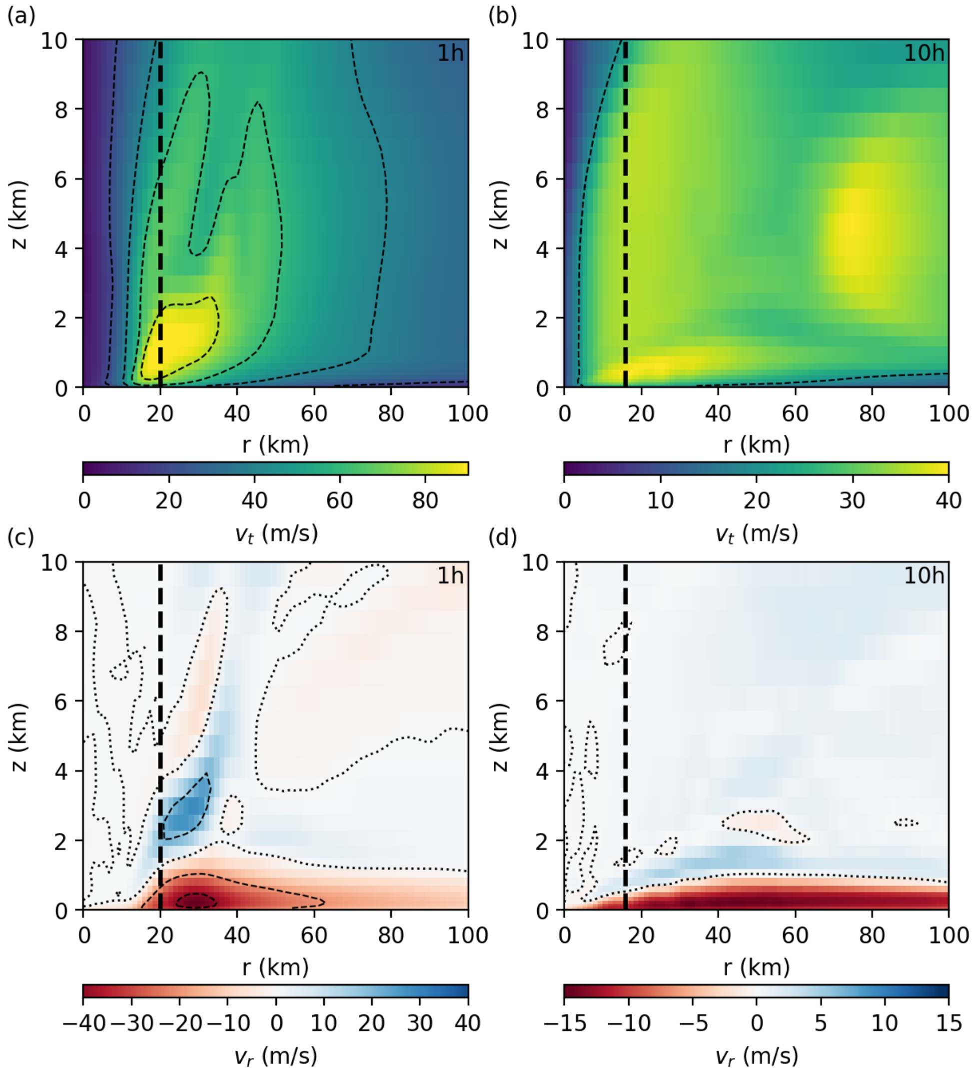

FIG. 7. Azimuthally averaged tangential wind speed, v_t and radial wind speed v_r, as a function of radius, r, and height, z, for the Control case 5 (a, c) 1 hour and (b, d) 10 hours after simulated landfall. Dotted lines are 0 contours, dashed contours show intervals of 20 m s^{-1}.

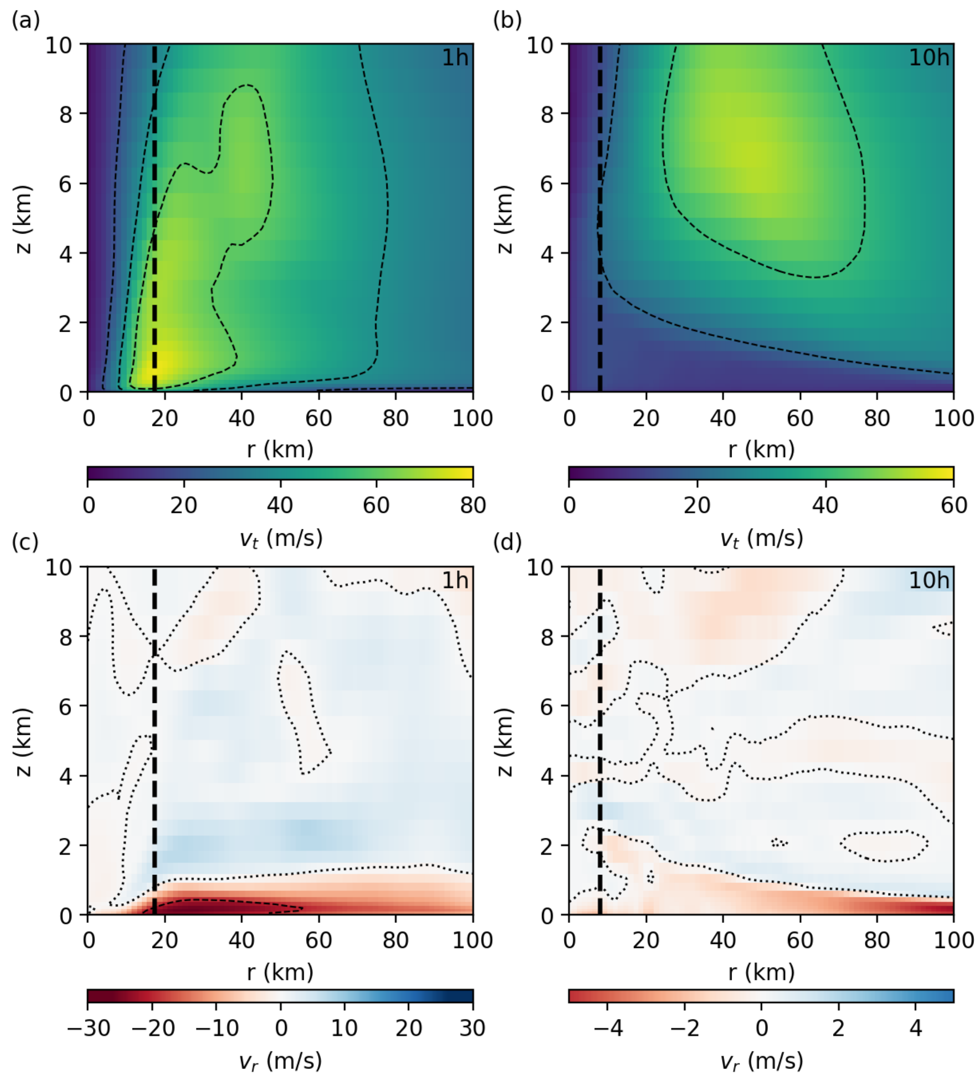

FIG. 8. As in Figure 7 but for the Dry case 5.

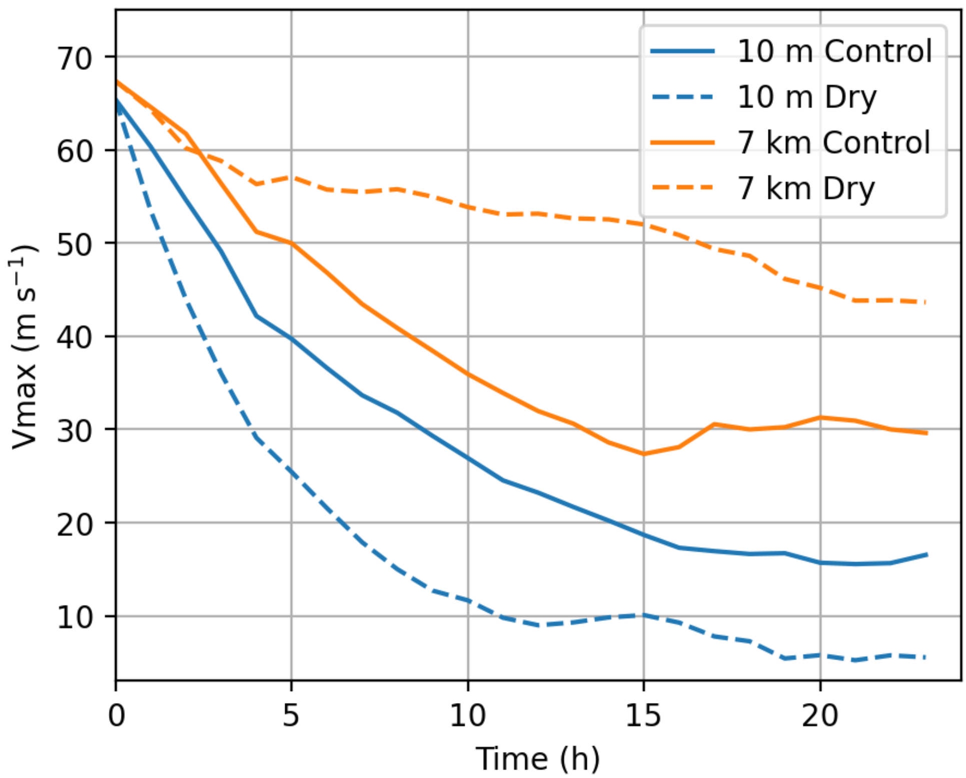

720 FIG. 9. Maximum wind speed, $Vmax$, as a function of time after simulated landfall at heights 10 m and 7 km
721 for the Control and Dry case 5.